A multi-scale two-level optimisation strategy integrating a global/local modelling approach for composite structures

Michele Iacopo Izzi[a], Marco Montemurro[a,*], Anita Catapano[b], Jérôme Pailhès[a]

[a]*Arts et Métiers ParisTech, I2M CNRS UMR 5295, F-33400 Talence, France*
[b]*Bordeaux INP, Université de Bordeaux, I2M CNRS UMR 5295, F-33400 Talence, France*

Abstract

In this work, a multi-scale optimisation strategy for the preliminary design of composite structures involving design requirements at different scales, is presented. Such a strategy, denoted as GL-MS2LOS, has been formulated by integrating a dedicated global-local (GL) modelling approach into the multi-scale two-level optimisation strategy (MS2LOS).

The GL-MS2LOS aims at proposing a very general formulation of the design problem, without introducing simplifying hypotheses and by considering, as design variables, the full set of geometric and mechanical parameters defining the behaviour of the composite structure at each pertinent scale. By employing a GL modelling approach, most of the limitations of well-established design strategies based on analytical or semi-empirical models are overcome.

The effectiveness of the presented GL-MS2LOS is proven on a meaningful study case: the least-weight design of a composite fuselage barrel of a wide-body aircraft undergoing various loading conditions and subject to requirements of different nature. Fully parametric global and local FE models are interfaced with an in-house metaheuristic algorithm to perform the optimisation. Refined local FE models are created only for critical regions of the structure, automatically detected during the global analysis, and linked to the global one thanks to the implementation of a sub-modelling approach. The whole process is completely automated and, once set, it does not need any further user intervention. The general nature of the GL-MS2LOS allows finding an optimised configuration characterised by a weight saving of 40% when compared to an optimised aluminium solution obtained through a similar GL optimisation strategy.

Keywords: Preliminary design, Optimisation, Global/local modelling approach, Composite material, Stiffened panel, Fuselage

---

*Corresponding author: Tel.: +33 556845422, Fax.: +33 540006964
Email address: marco.montemurro@ensam.eu; marco.montemurro@u-bordeaux.fr (Marco Montemurro)

1. Introduction

Aircraft structural design is mainly driven by lightness-related criteria while ensuring a set of performance-related requirements. Thanks to their high specific stiffness and strength properties, nowadays composite materials are massively used for primary aircraft components.

Composite materials can be suitably tailored to locally enhance stiffness and strength, thus offering a significant advantage over metals. Conversely, they introduce some specific phenomena, e.g. extension-bending coupling, delamination, free-edge stresses, different failure mechanisms, etc. Moreover, the design process of a composite structure is more difficult than that characterising a metallic one because of the high number of design variables involved at different scales.

In the aeronautical industry, decades of development of metallic aircraft design has led to the well-established "semi-monocoque" configuration as the conventional architecture for both fuselage and wing structures. As a consequence, this architecture has been extended to new composite solutions.

Due to their nature, aircraft structures made of composite materials present different working scales. At higher scales, the heterogeneity of the composite material can be neglected and only the overall anisotropic behaviour of the laminates is considered. Therefore, two working scales can be identified: the "global" macroscopic scale of the whole structure and the "local" macroscopic scale of the main components (e.g. the stiffened panels) constituting the structure. At these scales each composite part is modelled as an *equivalent anisotropic homogeneous continuum*.
At the lower scale, i.e. the mesoscopic scale of the elementary lamina composing each laminate, different phenomena take place that are related to the local stress field and to the specificity of the manufacturing process and that need different modelling strategies. Accordingly, the design of a composite structure must be formulated as a multi-scale optimisation problem.

The design-optimisation strategies available in the literature [1, 2] differ a) in the way the scale transition is handled, b) in the models and methods used to describe the main physical phenomena involved at different scales and c) in the algorithm employed to find an optimal solution.

Furthermore, most of the research works are applied to simple structures, like plates or simplified stiffened panels, that are the basic units of full-scale structures.

The so-called "bottom-up" approach was the first one to be used for design purposes. In this approach the plies orientation angles are directly taken as design variables, without using a dedicated multi-scale strategy. Typical examples are the works of Adali *et al.* [3], Haftka and Walsh [4], Le Riche and Hafka [5], Aymerich and Serra [6], Irisarri *et al.* [7, 8], Bisagni and Vescovini [9]. Most of these works deal with the problem of the buckling load and/or post-buckling stiffness maximisation with an assigned mass [3–6, 8], or the dual problem of minimisign the mass under constraints on the buckling strength [4, 7, 9], being the buckling phenomenon a main concern when dealing with the optimisation of thin-walled structures. Due to the discrete nature of the design variables and to the non-convexity of the problem, gradient-based algorithms cannot be used for the solution search and researchers have investigated and compared different meta-heuristics, including Genetic Algorithms (GAs), Integer Programming, Ant Colony Optimisation, Evolutionary Algorithms, searching for the most efficient choice, finally finding comparable results.

In each of the previous studies, the nature of the stack is set a priori and the orientation angles are limited to get values in a predefined set, usually the *canonical set* $\{0°, \pm 45°, 90°\}$, rarely an extended set like $\{0_2°, \pm 15°, \pm 30°, ..., 90_2°\}$. This is usually done both to explicitly

limit the extent of the design space and to (improperly) enforce some desired properties properties of the laminate, e.g. the use of symmetric stacking sequences, a sufficient but not necessary condition, to obtain membrane-bending uncoupling and the use of balanced stacks for orthotropic membrane stiffness matrix. Moreover, further empirical rules [10] (more or less justified) are usually employed as further design requirements. All these aspects contribute to strongly shrink the design domain leading the numerical tool to find only suboptimal solutions.

With the aim to reduce the number of design variables and to relax/suppress the non-convexity of the design problem, multi-scale optimisation (MSO) strategies for composite structures have been developed [1]. These strategies allow formulating and solving the optimisation problem at the macroscopic and mesoscopic scales in two sequential steps, resulting, thus, in a "top-down" design approach. Firstly, the structural optimisation is performed in terms of macroscopic properties of the laminate, through a suited representation. Secondly, the laminate lay-up design is carried out by retrieving suitable stacks corresponding to the optimum macroscopic properties of the laminate.

The most common MSO approach makes use of the well-known lamination parameters (LPs) coupled with the parameters of Tsai and Pagano [11]. These parameters [12, 13] unquestionably provide a compact representation of the stiffness tensors of the laminate, although they are not all tensor invariants [11]. Bloomfield *et al.* [14] presented a two-step MSO strategy for symmetric laminates made of a predefined set of ply orientations. The strategy is applied to the problem of mass minimisation of a simply supported multilayer plate under different loading conditions. Liu *et al.* [15] dealt with the maximisation of the laminate stiffness subject to a given set of optimisation constraints. During the first step, the optimisation problem is solved in the LPs space wherein the feasible region has been approximated by the one that can be obtained by considering only six different orientation angles. A suitable stack is then retrieved by solving a least-square problem. In [16] Herencia *et al.* employed an analogous strategy for the weight minimisation of composite panels with T-shaped stiffeners made of symmetric laminates with ply angles in the canonical set under strength, buckling and technological design requirements. Buckling constraints are computed employing an approximated semi-analytical approach. Stacking sequences found at the second step are slightly heavier and not always match the optimum LPs found at the first step.

An application of the LPs-based MSO on a full-scale structure can be found in the work of Bramsiepe *et al.* [17] where the least-weight design problem of a lifting system structure is solved. Failure, buckling and blending requirements are considered: the structure is made of symmetric laminates with ply angles varying with a step of $15°$. To evaluate the buckling load of the skin, the analytical formula for a simply supported plate under uniaxial load is used, retrieving the span-wise load component from a coarse global finite element model (GFEM). Moreover, the load redistribution is not directly considered, but the structural optimisation is performed under fixed loads at each iteration.

As it can be inferred from the previous works, the LPs-based MSO approach presents two main weaknesses: LPs are not tensor invariants, while not all Tsai and Pagano parameters are invariants; both LPs and Tsai and Pagano parameters have not an immediate physical meaning related to the elastic symmetries of the stiffness tensor. The latter is the main reason at the basis of the systematic use of simplifying hypotheses and rules on the nature of the stacking sequences used in the aforementioned works.

In order to reduce the computational cost of the whole optimisation process, in all the above studies, analytical (approximate) models are used for the assessment of the response of the structure. Accordingly, the main limitations in doing this are the lack of

accuracy and the limited applicability of such methods that rely on simplifying hypotheses, especially in terms of applied boundary conditions (BCs), often non-representative of real operative conditions.

To overcome these limitations, some authors proposed the use of improved semi-analytical formulations for composite stiffened panels based on the Rayleigh-Ritz method able to better describe the interaction between the skin and the stringers in the buckling phenomenon, but still neglecting the frames compliance and considering the structure infinitely periodic [9, 16]. In other works, surrogate models built from results of FE analyses are employed, but the problem of the representativeness of the employed BCs still persist and the phenomenon of mode switching can lead to a further inaccuracy in the evaluation of the buckling response [8, 18]. In particular, Vankan *et al.* [19], in a report of the Royal Netherlands Aerospace Centre (NLR) about the multi-scale optimisation of a composite fuselage barrel, compared the buckling load estimations, obtained by using a surrogate model built on the results of a parametric local FE model (LFEM) of an isolated stiffened panel subject to idealised BCs, to the results of GFEM analyses with the same refinement level. They showed the poor accuracy of the former model, highlighting the detrimental effect of the use of idealised BCs. The same problem is highlighted by Grihon *et al.* [20] in a review of the numerical optimisation methods developed/applied at AIRBUS. They identified the inaccuracy of some analytical models and the lack of load redistribution evaluation during the local scale optimisation as the main weaknesses (and the main causes of inconsistency) in the passage from the preliminary design phase to the detailed design.

Therefore, the use of a proper FE modelling strategy for both global and local scales phenomena assessment is preferable in these situations, but, as pointed out by Vekataraman and Hafka [21], even considering the increase of computational resources availability, its integration in optimisation strategies could still be difficult when large and complex structures described by many variables are considered.

In order to go beyond all the aforementioned issues, a dedicated global-local (GL) FE modelling approach is here integrated in the multi-scale two-level optimisation strategy (MS2LOS) for the preliminary optimisation of composite thin-walled structures. The resulting methodology is denoted via the acronym GL-MS2LOS. The GL-MS2LOS is based on the generalisation of the Verchery's polar method [22] to the case of higher-order equivalent single layer theories [23–25] as well as on the GA ERASMUS (EvolutionaRy Algorithm for optimiSation of ModUlar Systems) previously developed by Montemurro [26]. The GL-MS2LOS aims at proposing a very general formulation of the design problem, without introducing simplifying hypotheses and by considering, as design variables, the full set of geometric and mechanical parameters defining the behaviour of the composite structure at each characteristic scale (macroscopic and mesoscopic ones). Montemurro and his co-workers successfully applied the MS2LOS to the optimisation of various anisotropic structures (e.g. [26–31]) and have recently given a first experimental validation of its effectiveness [32].

GL modelling approaches allow to accurately asses phenomena involved at the local scale without the need of a refined GFEM that would require a strong computational effort to be integrated into an optimisation strategy. Instead, refined LFEMs with realistic BCs derived from a coarse GFEM analysis are used in the proposed GL-MS2LOS. Among the different GL approaches available in the literature, the sub-modelling technique [33–36] is employed in this work. In the usual work-flow of the sub-modelling GL approach, firstly a low fidelity linear analysis on a GFEM with a coarse mesh is run to identify one or more zones of interest (ZOIs). Then a refined LFEM is created for each ZOI where a subsequent analysis is performed imposing displacements provided by the GFEM as BCs. Moreover,

iterative stages can be added if the stress redistribution due to local effects is considered non-negligible.

The GL modelling approach is integrated into the first-level problem formulation of the MS2LOS. Here the MS2LOS focuses on the structural optimisation and the design variables are the polar parameters of each laminate composing the structure as well as other geometrical quantities. No assumption is made on the nature of the stacking sequences and desired elastic symmetries of the laminates are naturally got through an efficient use of the polar parameters. In this way, no restrictions are imposed on the design space and, consequently, a true global optimum can be found. All the design criteria and requirements involved into the problem formulation are evaluated by means of fully parametric GFEM and LFEMs. Computational time is kept as low as possible by verifying local responses only on the most critical ZOIs. To this purpose, pertinent design criteria are introduced into the GFEM to automatically identify the ZOIs and build the related refined LFEMs. Moreover, because for each set of design variables both GFEM and LFEMs are generated and no local-only optimisation is performed, there is no problem related to missed load redistribution evaluation.

The second level of the MS2LOS, as described in [23–32], is devoted to the stacking sequences retrieval. This paper will focus only on the first level of the MS2LOS because the procedure relative to the second level remains unchanged when compared to the afore-mentioned works.

The effectiveness of the GL-MS2LOS is proven on a meaningful real-world engineering problem: the least-weight design of a composite fuselage barrel belonging to the aft part of a wide-body aircraft that undergoes multiple loading conditions and subject to constraints of different nature.

The paper is organised as follows. A general description of the design problem, the underlying hypotheses and the driving design criteria are given in Sec. 2. The fundamentals of the polar method extended to the case of the First-order Shear Deformation Theory (FSDT) are provided in Sec. 3. The mathematical formulation of the multi-scale design problem and the adopted numerical strategy are discussed in Sec. 4. The details on the FE models and the implementation of the GL approach are presented in Sec. 5. Numerical results are shown in Sec. 6. Finally, Sec. 7 ends the paper with some conclusions and perspectives.

2. Least-weight design of a composite fuselage barrel

2.1. Problem description

The GL-MS2LOS presented in this study is applied to the least-weight design of a composite fuselage barrel of a wide-body aircraft. The fuselage barrel has a circular cross-section and is located between the wing rear spar and the tail, as shown in Fig. 1. The fuselage barrel is clamped at the rear spar section (section A) and loads coming from the tail are applied to section B. Payload weight and pressurisation are also taken into account. More details on the BCs and the load cases considered in the design process are given in Secs. 2.2 and 2.3.

The main geometrical parameters of the fuselage barrel are reported in Tab. 1. The generic stiffened panel geometry considered in this study is shown in Fig. 2. It is a full composite assembly made of hat-shaped stringers and floating frames with a Z-shaped cross-section. Stringers are attached to the skin by means of "shear tie" components, whilst no "stringer tie" or "tear strap" components are present. Metallic floor beams
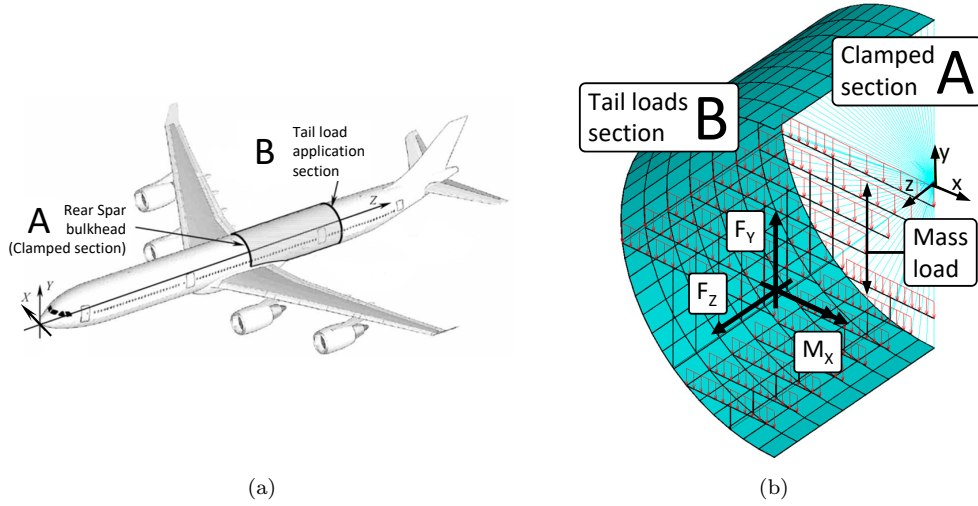
5

Figure 1: Location of the fuselage barrel [37] (a) and detail of the applied BCs (b).

Component	Value
Fuselage diameter [mm]	5640
Number of bays	7
Bay pitch [mm]	500
Upper-deck floor vertical position [mm] [†]	−152
Lower-deck floor vertical position [mm] [†]	−2130
Struts position on upper-deck floor beam [*]	1/3
Struts position on lower-deck floor beam [*]	1/4

[†] Referred to the horizontal axis through the geometrical centre of the fuselage cross-section.
[*] Normalised with the floor beam length and referred to the aircraft symmetry plane.

Table 1: Main geometrical parameters of the fuselage barrel.

with an I-shaped cross-section and metallic tubular struts complete the set of structural components.

The main structural components are made of laminates. The elementary lamina is the unidirectional T300/5208 carbon/epoxy pre-preg, having a linear elastic transversely isotropic behaviour. The metallic components are made of 2024-T3 aluminium alloy, with a linear elastic isotropic behaviour. The mechanical and physical properties of these materials are reported in Tabs. 2 and 3; the meaning of the polar parameters present in these tables is clarified in Sec. 3.

A reference solution (REF) has been obtained by the authors by optimising an analogous metallic fuselage barrel, entirely made of the 2024-T3 aluminium alloy and subject to an equivalent set of design criteria, with a strategy employing a global/local modelling approach similar to the MSO strategy presented in this work. The data necessary to define the reference solution can be found in Tab. 4; the meaning of some of these parameters is explained in Sec. 4.1.

2.2. Hypotheses and design criteria

The MS2LOS here presented is framed into the preliminary design phase of aircraft structures. During this phase, tents of load cases (LCs) are assessed to properly design the main components of the structure in order to comply with certification specifications [40]. Such LCs are the result of a combination of basic loading conditions (BLCs) of different
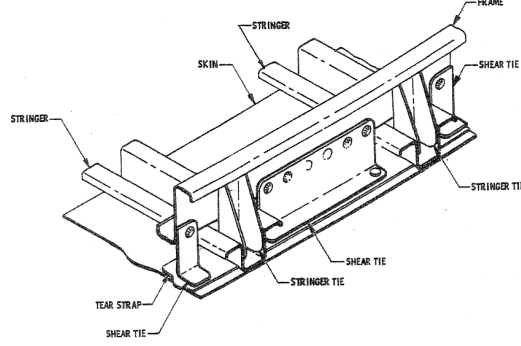
Figure 2: Architecture of the stiffened panel.

Technical constants		Polar parameters of $\left[Q^{\mathrm{in}}\right]^{a}$		Polar parameters of $[Q^{\mathrm{out}}]^{b}$	
E_1 [MPa]	181000	T_0 [MPa]	26899	T [MPa]	5398
E_2 [MPa]	10300	T_1 [MPa]	24710	R [MPa]	1772
G_{12} [MPa]	7170	R_0 [MPa]	19729	Φ [deg]	90
ν_{12}	0.27	R_1 [MPa]	21426		
ν_{23}	0.42	Φ_0 [deg]	0		
		Φ_1 [deg]	0		
Engineering strengths		Pol. par. of $\left[G^{\mathrm{in}}\right]^{c}$		Pol. par. of $\left[G^{\mathrm{out}}\right]^{d}$ and $\left\{g^{\mathrm{in}}\right\}^{e}$	
X = X' [MPa]	1500	Γ_0^{in} [MPa]	7531	Γ^{out} [MPa]	11076
Y = Z [MPa]	40	Γ_1^{in} [MPa]	2114	Λ^{out} [MPa]	38
Y' = Z' [MPa]	246	Λ_0^{in} [MPa]	3587	Ω^{out} [deg]	90
Q = Q' [MPa]	36	Λ_1^{in} [MPa]	1603	γ^{in} [MPa]	137
R = R' [MPa]	68	Ω_0^{in} [deg]	90	λ^{in} [MPa]	79
S = S' [MPa]	68	Ω_1^{in} [deg]	0	ω^{in} [deg]	90
Density and thickness					
ρ_{c} [g/cm^3]	1.6				
t_{ply} [mm]	0.125				

^{a} In-plane reduced stiffness matrix of the ply.
^{b} Out-of-plane shear stiffness matrix of the ply.
^{c} In-plane strength matrix of the ply.
^{d} Out-of-plane strength matrix of the ply.
^{e} In-plane strength vector of the ply.

Table 2: Material properties of the unidirectional T300/5208 carbon/epoxy ply [38].

nature, e.g. flight loads due to symmetrical manoeuvres, to asymmetrical ones or to gusts, ground loads, pressurisation, etc. In this work, only a sub-set of LCs, presented in Sec. 2.3, is considered. Moreover, for each LC, the material behaviour is supposed linear elastic and the FE analyses are carried out by assuming small displacements and strains.

Concerning the modelling of the structural components, the following simplifications have been introduced:

1. In agreement with the preliminary design framework, only major components of the structure are modelled (i.e. skin, frames, stringers, floor beams and struts).

2. Floor beams and struts have a predefined geometry which is kept unchanged during optimisation.

3. The elastic response of the laminates is modelled according to the FSDT.

4. Perfect bonding is assumed at the interface of the structural elements and between plies.

Propriety	Value
Young's modulus, E [MPa]	72395
Poisson's ratio, ν	0.33
Tensile yield stress, σ_y [MPa]	290
Tensile ultimate stress, σ_u [MPa]	434
Density, ρ_{Al} [g/cm^3]	2.78

Table 3: Material properties of 2024-T3 aluminium alloy [39].

Component	Value		
Frame flange width (w_3^{Fr}) [mm]	20.0		
Frame web height (w_3^{Fr}) [mm]	81.0		
Frame thickness (t^{Fr}) [mm]	1.0		
Cabin floor beams web height [mm]	240.0		
Cabin floor beams flange width [mm]	156.0		
Cabin floor beams thickness [mm]	2.5		
Cargo floor beams web height [mm]	180.0		
Cargo floor beams flange width [mm]	60.0		
Cargo floor beams thickness [mm]	1.5		
Struts external diameter [mm]	21.5		
Struts internal diameter [mm]	15.5		
Component	Top	Lateral	Bottom
Stringer free flanges width (w_1^{St}) [mm]	5.0	5.0	21.0
Stringer bonded flange width (w_3^{St}) [mm]	40.6	24.5	31.0
Stringer height (w_4^{St}) [mm]	19.0	38.0	45.5
Stringer thickness (t^{St}) [mm]	1.1	1.0	1.4
Skin thickness (t^{Sk}) [mm]	1.8	3.0	3.6
Skin-panels count (n^{Sk}) [-]	36	24	18

Table 4: Geometrical parameters of the reference solution REF.

5. Connection zones (e.g. floor beams to frames or skin to skin) and opening/cut-out in the skin are not explicitly modelled.

Three main groups of criteria can be identified for the preliminary design phase, i.e. criteria related to: a) static loads, b) fatigue loads and c) aeroelasticity phenomena. This work focuses only on design criteria related to static loads.

Certification specifications [40] identify two types of static design loads: *limit loads* (LLs) and *ultimate loads* (ULs). LLs are the maximum loads expected in service that the structure must withstand without detrimental permanent deformations. ULs are equal to limit loads multiplied by a prescribed factor of safety (usually 1.5). The structure must withstand ULs without failure for at least 3 seconds. For instance, for the wide-body civil aircraft class, LLs in symmetrical manoeuvres occur at load factors (the ratio of the aerodynamic force component normal to the longitudinal axis of the aeroplane to its weight) $n_g = 2.5$ and $n_g = -1$.

The following set of design criteria (DCs) is integrated in the design process.

DC1 The global stiffness of the structure must be greater than the stiffness of REF.

DC2 No failure must occur under loads up to ULs.

DC3 No buckling must occur in the stiffened panels under ULs (no-buckling design approach).

DC4 Only manufacturable solutions are considered.

DC5 The laminates composing the structures have a fully orthotropic (membrane and bending) quasi-homogeneous macroscopic behaviour.

DC2 is verified at the laminate-level by means of a suited failure criterion ([41], further details in Sec. 3.2).

2.3. Load cases

Five LCs are defined by linear superposition of two BLCs: a cruise loading condition (load factor $n_g = 1$) without pressurisation, identified as BLC_{1g}, and a pressurisation loading condition, identified as BLC_p. In both BLCs, fuselage sections A and B are modelled as rigid and BCs are applied to their centres: section A is always clamped, whilst pertinent tail forces and moments are applied at section B.

Under BLC_{1g}, payload weight is applied as a distributed load on floor beams. Structural mass is considered by applying additional loads on the upper-deck floor beams, on the basis of statistical estimated structural weight. Tail loads are computed in such a way to obtain in the check zone (i.e. the middle bay of the fuselage barrel) a maximum bending moment $M_x = 5.0 \cdot 10^6$ Nm and a maximum vertical shear force $F_y = -3.7 \cdot 10^5$ N. A good estimation of the loading condition at a different value of the load factor is obtained by scaling BLC_{1g} by that value.

When using BLC_p, the effect of the maximum operating differential pressure (corresponding to the maximum relief valve setting) is taken into account as internal pressure on the skin plus an equivalent longitudinal force applied to section B of the fuselage barrel. By scaling BLC_p, the effect of different values of differential pressure can be assessed.

Data used for defining BLC_{1g} and BLC_p are reported in Tab. 5. The five considered LCs are defined in Tab. 6 in which, for each LC, the related design criterion is also indicated. Aerodynamics loads on the fuselage have been neglected.

Load	BLC_{1g}	BLC_p
Upper-deck floor beam total load [N]	10000	-
Lower-deck floor beam total load [N]	5000	-
Bending moment M_x at section "B" [Nm]	$4.305 \cdot 10^6$	-
Vertical shear force F_y at section "B" [N]	$-3.1 \cdot 10^5$	-
Differential pressure [MPa]	-	0.068
Longitudinal force F_z [N] [†]	-	$1.7 \cdot 10^6$

[†] Equivalent to internal pressure times fuselage cross-section area.

Table 5: Basic loading conditions data.

LC	BLC_{1g} factor	BLC_p factor	DC
1	1.00	1.00	DC1
2	3.75	1.00	DC2
3	-1.50	1.00	DC2
4	3.75	0	DC3
5	-1.50	0	DC3

Table 6: Load cases definition and associated design criterion.

3. The polar analysis of laminates

In this section, the fundamentals of the polar analysis of laminates stiffness and strength matrices are provided; for a deeper insight in the matter, the reader is addressed to [23, 24, 41, 42].

Verchery's polar method [22] allows for expressing any n-rank plane tensor through a set of tensor invariants. In the context of this work, two types of tensors are relevant:

second-rank symmetric plane tensors Z_{ij} (with $i, j = 1, 2$) and fourth-rank elasticity-like (i.e. having both major and minor symmetries) plane tensors L_{ijkl} (with $i, j, k, l = 1, 2$). They can be expressed in terms of their polar parameters as:

$$
\begin{aligned}
Z_{11} &= &+ \, T & &+ \, R\cos 2\Phi &\quad, \\
Z_{12} &= & & &+ \, R\sin 2\Phi &\quad, \\
Z_{22} &= &+ \, T & &- \, R\cos 2\Phi &\quad,
\end{aligned}
\tag{1}
$$

and

$$
\begin{aligned}
L_{1111} &= &+ \, T_0 &+ 2T_1 &+ R_0\cos 4\Phi_0 &+ 4R_1\cos 2\Phi_1 &\quad, \\
L_{1122} &= &- \, T_0 &+ 2T_1 &- R_0\cos 4\Phi_0 & &\quad, \\
L_{1112} &= & & &+ R_0\sin 4\Phi_0 &+ 2R_1\sin 2\Phi_1 &\quad, \\
L_{2222} &= &+ \, T_0 &+ 2T_1 &+ R_0\cos 4\Phi_0 &- 4R_1\cos 2\Phi_1 &\quad, \\
L_{2212} &= & & &- R_0\sin 4\Phi_0 &+ 2R_1\sin 2\Phi_1 &\quad, \\
L_{1212} &= &+ \, T_0 & &- R_0\cos 4\Phi_0 & &\quad.
\end{aligned}
\tag{2}
$$

In Eqs. (1) and (2), T, T_0 and T_1 are the isotropic moduli, R, R_0 and R_1 are the anisotropic ones, while Φ, Φ_0 and Φ_1 are the polar angles. Among them T, R and T_0, T_1, R_0, R_1, $\Phi_0 - \Phi_1$ are tensor invariants, while Φ and one of the two polar angles, Φ_0 or Φ_1, can be arbitrarily chosen to fix the reference frame, for second and fourth order tensors, respectively.

One of the main advantages provided by the polar formalism is that requirement on elastic symmetries of the tensor can be translated into simple algebraic conditions on the related polar parameters. For example, the ordinary orthotrophy of a fourth-rank elasticity-like tensor corresponds to the condition:

$$
\Phi_0 - \Phi_1 = K \cdot \pi/4 \quad \text{with } K = 0, 1.
\tag{3}
$$

For more details about the elastic symmetries and their expression in terms of polar parameters see [23, 24].

3.1. The polar formalism for the laminate stiffness matrices

In the background of the FSDT [43], the constitutive law of a laminate (expressed within its global frame) reads:

$$
\left\{
\begin{array}{c}
\{N\} \\
\{M\} \\
\{F\}
\end{array}
\right\}
=
\left[
\begin{array}{ccc}
[A] & [B] & 0 \\
[B] & [D] & 0 \\
0 & 0 & [H]
\end{array}
\right]
\left\{
\begin{array}{c}
\{\varepsilon_0\} \\
\{\chi_0\} \\
\{\gamma_0\}
\end{array}
\right\}
,
\tag{4}
$$

where $[A]$, $[B]$ and $[D]$ are the 3×3 membrane, membrane/bending coupling and bending stiffness matrices of the laminate, while $[H]$ is the 2×2 out-of-plane shear stiffness matrix. $\{N\}$, $\{M\}$ and $\{F\}$ are the vectors of membrane forces, bending moments and shear forces per unit length, respectively, whilst $\{\varepsilon_0\}$, $\{\chi_0\}$ and $\{\gamma_0\}$ are the vectors of in-plane strains, curvatures and out-of-plane shear strains of the laminate middle plane, respectively.

Matrices $[A]$, $[B]$, $[D]$ and $[H]$, can be normalised to have the same units (i.e. MPa) as:

$$
[A^*] = \frac{1}{t}[A] \ , \quad [B^*] = \frac{2}{t^2}[B] \ , \quad [D^*] = \frac{12}{t^3}[D] \ , \quad [H^*] = \frac{1}{t}[H]
\tag{5}
$$

As deeply discussed in [23, 24], $[A^*]$, $[B^*]$ and $[D^*]$ behave like tensor **L** of Eq. (2) and

10

[H*] behaves like tensor **Z** of Eq. (1), therefore it is possible to express the Cartesian components of these matrices in terms of polar parameters, for an overall number of 21 parameters. It can be proven that, if the in-plane reduced stiffness matrix [Q^{in}] and the out-of-plane shear stiffness matrix [Q^{out}] of the elementary ply are known, only 12 polar parameters are independent (the relation between matrices [A], [B], [D] and [H] and matrices [Q^{in}] and [Q^{out}] can be found in Appendix A). Moreover, if, according to DC5, the hypothesis of fully orthotropic quasi-homogeneous laminate is introduced, i.e.

$$[A^*] = [D^*] \;, \qquad [B^*] = [0] \;, \qquad \Phi_0^{A*} - \Phi_1^{A*} = K \cdot \pi/4 \;, \tag{6}$$

the overall number of independent polar parameters reduces to only three: the anisotropic polar moduli $R_{0K}^{A*} = (-1)^{K^{A*}} \cdot R_0^{A*}$, R_1^{A*} and the polar angle Φ_1^{A*} (this last representing the orientation of the main orthotropy axis) of matrix [A*]. For more details on the polar formalism and its application in the context of the FSDT the reader is addressed to [23, 24, 42].

3.2. The polar formalism for the laminate strength

For the application of DC2, a general laminate-level failure criterion formulated by Catapano and Montemurro [41] is employed. This criterion represents a general unified formula including various phenomenological failure criteria. The formulation used in this work is based on the Tsai-Wu (TW) failure criterion [44] that, in matrix notation, reads

$$F_{TW} = \{\sigma\}^T [F] \{\sigma\} + \{\sigma\}^T \{f\} \leq 1 \;, \tag{7}$$

where $\{\sigma\}$ is the stress vector in Voigt's notation, while [F] and $\{f\}$ depend on the lamina strength properties [44].

By introducing the FSDT hypothesis of null out-of-plane stress, by separating the in-plane and out-of-plane contributions and by using the Hooke's law, Eq. (7) can be rewritten in terms of strain, obtaining:

$$F_{TW} = \left\{\varepsilon^{in}\right\}^T \left[G^{in}\right] \left\{\varepsilon^{in}\right\} + \left\{\varepsilon^{out}\right\}^T \left[G^{out}\right] \left\{\varepsilon^{out}\right\} + \left\{\varepsilon^{in}\right\}^T \left\{g^{in}\right\} \leq 1 \;, \tag{8}$$

where $\left[G^{in}\right]$ and $\left[G^{out}\right]$ can be considered as the strength matrices of the constitutive ply. Finally, making use of the FSDT kinematics, one can express Eq. (8) in terms of the laminate middle plane strains

$$\begin{aligned} F_{TW} = \{\varepsilon_0\}^T \left[G^{in}\right] \{\varepsilon_0\} + z^2 \{\chi_0\}^T \left[G^{in}\right] \{\chi_0\} + 2z \{\varepsilon_0\}^T \left[G^{in}\right] \{\chi_0\} + \\ \ldots + \{\gamma_0\}^T \left[G^{out}\right] \{\gamma_0\} + \{\varepsilon_0\}^T \left\{g^{in}\right\} + z \{\chi_0\}^T \left\{g^{in}\right\} \leq 1 \;. \end{aligned} \tag{9}$$

The *laminate failure index* is calculated by averaging Eq. (9) through the thickness of the laminate, t:

$$F_{TW}^{lam} = \frac{1}{t} \int_t F_{TW}(z) \, dz \leq 1 \quad . \tag{10}$$

Eq. (10) simplifies to:

$$\begin{aligned} F_{TW}^{lam} = \frac{1}{t} \Big(\{\varepsilon_0\}^T [G_A] \{\varepsilon_0\} + \{\chi_0\}^T [G_D] \{\chi_0\} + \{\varepsilon_0\}^T [G_B] \{\chi_0\} + \\ + \{\gamma_0\}^T [G_H] \{\gamma_0\} + \{\varepsilon_0\}^T \{g_A\} + \{\chi_0\}^T \{g_D\} \Big) \leq 1 \;. \end{aligned} \tag{11}$$

The details of the algebric manipulations to get Eq. (11) can be found in [41]. Matrices $[G_A]$, $[G_B]$, $[G_D]$ and $[G_H]$ and vectors $\{g_A\}$ and $\{g_D\}$ represent the laminate strength matrices and vectors. In particular, the four matrices can be seen as the strength counterpart of stiffness matrices $[A]$, $[B]$, $[D]$ and $[H]$ in the FSDT framework (the definition of these matrices and vectors is reported in Appendix A). As done for the laminate stiffness matrices, normalised strength matrices and vectors can be defined as follows:

$$[G_A^*] = \frac{1}{t}[G_A] \ , \quad [G_B^*] = \frac{2}{t^2}[G_B] \ , \quad [G_D^*] = \frac{12}{t^3}[G_D] \ , \quad [G_H^*] = \frac{1}{t}[G_H] \ ,$$
$$\{g_A^*\} = \frac{1}{t}\{g_A\} \ , \quad \{g_D^*\} = \frac{2}{t^2}\{g_D\} \ . \tag{12}$$

The polar formalism can be applied to these matrices and vectors too.

Catapano and Montemurro showed that, when the strength properties of the constitutive ply (i.e. matrices $[G^{in}]$ and $[G^{out}]$ and vector $\{g^{in}\}$, and their polar parameters) are known, the laminate strength matrices and vectors can be expressed in terms of the stiffness polar parameters described in Sec. 3.1. This means that polar parameters describing the laminate stiffness matrices and those describing strength matrices and vectors are not independent. Accordingly, only one of these two sets of polar parameters must be included among the design variables of the problem at hand because the remeaning set can be easily derived by using the formulae provided in [41]. When a fully orthotropic quasi-homogeneous laminate is considered, the overall number of independent polar parameters describing its behaviour (in terms of both stiffness and strength) remains three: the anisotropic polar moduli $R_{0K}^{A^*}$ and $R_1^{A^*}$ and the polar angle $\Phi_1^{A^*}$ of both matrices $[A^*]$ and $[D^*]$, or, alternatively, their counterpart of matrices $[G_A^*]$ and $[G_D^*]$. More details on the polar analysis of laminates strength and on the correlation between laminate strength and stiffness polar parameters can be found in [41].

4. Mathematical formulation of the optimisation problem

4.1. Design variables

Both mechanical and geometrical design variables are considered in this study. Stringers, frames, and shear ties sections are assumed to be obtained by folding fully orthotropic quasi-homogeneous laminates. The design variables can be grouped with respect to the component they are referred to.

Stringers and skin. Three circumferential sectors are identified as in Fig. 3: "top", "lateral" and "bottom". For each sector:

- the stringers cross-section is hat-shaped; four variables, $w_1^{St}, w_3^{St}, w_4^{St}$ and t^{St}, are needed to describe its geometry (Fig. 4a) and two variables, i.e. the polar parameters $R_{0K}^{A^*-St}$ and $R_1^{A^*-St}$ are needed to describe the mechanical properties;

- the skin is characterised by two geometrical variables, i.e. the thickness t^{Sk} and the number n^{Sk} of sub-regions between two consecutive frames and stringers (hereafter *skin-panels*) within the sector and two mechanical design variables, i.e. the polar parameters $R_{0K}^{A^*-Sk}$ and $R_1^{A^*-Sk}$;

Frame/shear-tie assembly. Identical frames having a "Z"-shaped cross-section with "L" shear-tie are considered: three variables, w_1^{Fr}, w_3^{Fr} and t^{Fr}, are needed to geometrically describe the assembly (Fig. 4b). The distance between the floating frame

and the fuselage skin depends on the maximum height of the stringers cross-sections according to the formula

$$c^{\text{Fr}} = \max_i \ w_4^{\text{St}-i} + 2\text{mm} , \quad \text{with } i = \text{Top, Lat, Bot.}$$

The frames and the shear-ties are made of identical laminates whose mechanical properties are described by the two polar parameters $R_{0K}^{\text{A}*-\text{Fr}}$ and $R_1^{\text{A}*-\text{Fr}}$, which represent the mechanical design variables.

Regarding the orientation of the main orthotropy axis of the laminates composing the different components (represented by the polar angles $\Phi_1^{\text{A}*-j}$ with $j = \text{St, Sk, Fr}$), it has been set equal to $0°$ within suited local reference systems of the laminates, in such a way to align it with the fuselage longitudinal axis for stringers and skin and to follow the hoop direction for the frames.

Of course, the laminates thickness must be a multiple of the elementary ply thickness, thus the number of plies $n_{\text{ply}}^j = t^j/t_{\text{ply}}$ (with $j = \text{St, Sk, Fr}$) is used as a dimensionless design variable.

Finally, the variables $R_{0K}^{\text{A}*-j}$ and $R_1^{\text{A}*-j}$ are replaced by their dimensionless counterpart (denoted as ρ_0^j and ρ_1^j) obtained as follows:

$$\rho_0^j = R_{0K}^{\text{A}*-j}/R_0 , \quad \rho_1^j = R_1^{\text{A}*-j}/R_1 , \quad \text{with } j = \text{St, Sk, Fr,} \tag{13}$$

where R_0 and R_1 are the anisotropic moduli of the in-plane reduced stiffness matrix of the elementary ply given in Tab. 2.
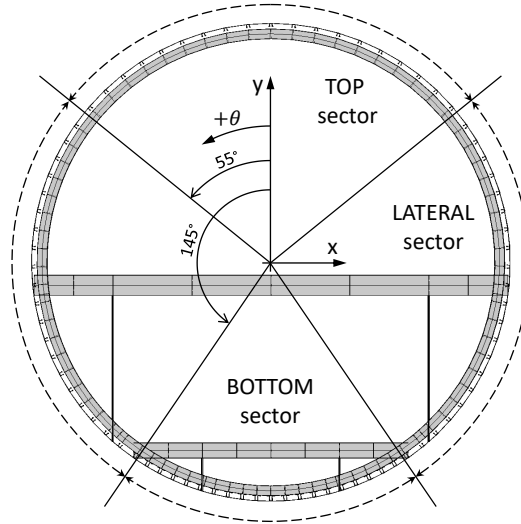

Figure 3: Fuselage cross-section.

All the aforementioned design variables are collected into the vector $\boldsymbol{\xi}$. It is noteworthy that frame pitch, floor beams and struts geometry have not been considered among the problem design variables, rather they have been set equal to the reference values of the REF as reported in Tabs. 1 and 4.
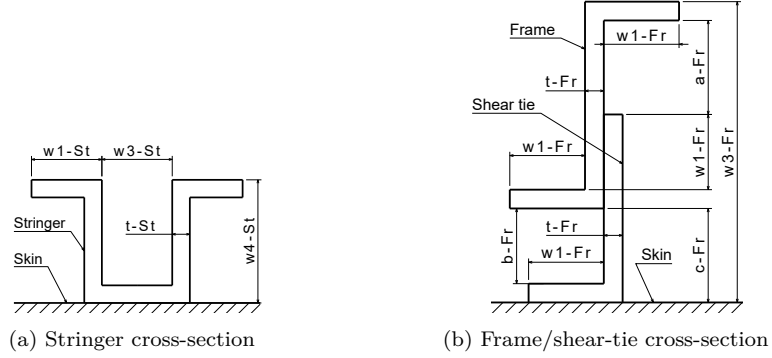
(a) Stringer cross-section   (b) Frame/shear-tie cross-section

Figure 4: Stringers and frame/shear-tie assembly cross-sections variables definition.

4.2. Objective and constraint functions

The goal of the optimisation is the minimisation of the total mass of the fuselage barrel which can be easily expressed as

$$M\left(\boldsymbol{\xi}\right) = V_{\mathrm{c}}\left(\boldsymbol{\xi}\right) \cdot \rho_{\mathrm{c}} + M_{\mathrm{Al}} \, , \tag{14}$$

where $V_{\mathrm{c}}\left(\boldsymbol{\xi}\right)$ is the total volume of the composites constituting the structure, ρ_{c} is density of the composite material, as defined in Tab. 2, and M_{Al} is the mass of the aluminium components (i.e. floor beams and struts).

As far as design requirements are concerned, one or more constraint functions are defined for DC1-4, introduced in Sec. 2.2. DC5 has a direct effect on the choice of the mechanical design variables as explained in Sec. 3.1.

DC1 is formulated as a couple of constraints on the vertical displacement δ_{y} and on the rotation θ_{x} of the centre of section B when LC1 is considered. These constraints read

$$\begin{aligned} g_1\left(\boldsymbol{\xi}\right) &= \left(\delta_{\mathrm{y}}\left(\boldsymbol{\xi}\right) - \delta_{\mathrm{y}}^{\mathrm{REF}}\right)/\delta_{\mathrm{y}}^{\mathrm{REF}} \leq 0 \, , \\ g_2\left(\boldsymbol{\xi}\right) &= \left(\theta_{\mathrm{x}}\left(\boldsymbol{\xi}\right) - \theta_{\mathrm{x}}^{\mathrm{REF}}\right)/\theta_{\mathrm{x}}^{\mathrm{REF}} \leq 0 \qquad \text{at LC1.} \end{aligned} \tag{15}$$

In Eq. (15), $\delta_{\mathrm{y}}^{\mathrm{REF}} = -3.85$ mm and $\theta_{\mathrm{x}}^{\mathrm{REF}} = 0.061\,^{\circ}$ are the vertical displacement and rotation of the centre of section B evaluated for REF.

DC2 is applied through the evaluation of the maximum laminate failure index $\left\langle F_{\mathrm{TW}}^{\mathrm{lam}} \right\rangle$ of Eq. (11) averaged over the area of each skin-panel (ω_j) belonging to the check zone of each circumferential sector (see Secs. 4.1 and 5 for more details) in order to neglect the effect of local stress/strain concentrations that could be strongly affected by the accuracy of the FE model and that constitute the object of the detailed design phase (performed after the preliminary design phase).

Such value has to be lower than 1 with a factor of safety $\mathrm{F_S} = 2$ under both LC2 and LC3.

14

Therefore, the related constraint inequalities are:

$$g_3\left(\boldsymbol{\xi}\right) = \left(\mathrm{F_S} \cdot \max_{\Omega_{\mathrm{Top}}} \left\langle F_{\mathrm{TW}}^{\mathrm{lam}}\left(\boldsymbol{\xi}\right) \right\rangle_{\omega_j}\right) - 1 \le 0 \quad \text{at LC2,}$$

$$g_4\left(\boldsymbol{\xi}\right) = \left(\mathrm{F_S} \cdot \max_{\Omega_{\mathrm{Lat}}} \left\langle F_{\mathrm{TW}}^{\mathrm{lam}}\left(\boldsymbol{\xi}\right) \right\rangle_{\omega_j}\right) - 1 \le 0 \quad \text{at LC2,}$$

$$g_5\left(\boldsymbol{\xi}\right) = \left(\mathrm{F_S} \cdot \max_{\Omega_{\mathrm{Bot}}} \left\langle F_{\mathrm{TW}}^{\mathrm{lam}}\left(\boldsymbol{\xi}\right) \right\rangle_{\omega_j}\right) - 1 \le 0 \quad \text{at LC2,}$$

$$g_6\left(\boldsymbol{\xi}\right) = \left(\mathrm{F_S} \cdot \max_{\Omega_{\mathrm{Top}}} \left\langle F_{\mathrm{TW}}^{\mathrm{lam}}\left(\boldsymbol{\xi}\right) \right\rangle_{\omega_j}\right) - 1 \le 0 \quad \text{at LC3,}$$

$$g_7\left(\boldsymbol{\xi}\right) = \left(\mathrm{F_S} \cdot \max_{\Omega_{\mathrm{Lat}}} \left\langle F_{\mathrm{TW}}^{\mathrm{lam}}\left(\boldsymbol{\xi}\right) \right\rangle_{\omega_j}\right) - 1 \le 0 \quad \text{at LC3,}$$

$$g_8\left(\boldsymbol{\xi}\right) = \left(\mathrm{F_S} \cdot \max_{\Omega_{\mathrm{Bot}}} \left\langle F_{\mathrm{TW}}^{\mathrm{lam}}\left(\boldsymbol{\xi}\right) \right\rangle_{\omega_j}\right) - 1 \le 0 \quad \text{at LC3.}$$

(16)

In Eq. (16), $\Omega_i = \sum_{j=1}^{N_i} \omega_j$ with $i = \mathrm{Top}$, Lat, Bot represents the i-th portion of the check zone of the fuselage barrel, whilst ω_j is the j-th skin-panel belonging to this region (more details are given in Sec. 5).

The requirement DC3 can be opportunely expressed by means of three optimisation constraints. For each circumferential sector, ULs are applied and the most critical stiffened panel (composed of three stringers and two frames, as discussed in Sec. 5) in the check zone is identified. An eigenvalue buckling analysis is then performed on this panel. The first buckling eigenvalue has to be higher than 1 with a factor of safety $\mathrm{F_S} = 1.1$ (more details on this point are given in Sec. 5). The related constraints read

$$g_9\left(\boldsymbol{\xi}\right) = 1.1 - \lambda^{\mathrm{Top}}\left(\boldsymbol{\xi}\right) \le 0 \quad \text{at LC5,}$$

$$g_{10}\left(\boldsymbol{\xi}\right) = 1.1 - \lambda^{\mathrm{Lat}}\left(\boldsymbol{\xi}\right) \le 0 \quad \text{at LC4,}$$

$$g_{11}\left(\boldsymbol{\xi}\right) = 1.1 - \lambda^{\mathrm{Bot}}\left(\boldsymbol{\xi}\right) \le 0 \quad \text{at LC4.}$$

(17)

The application of DC4 involves both mechanical and geometrical manufacturability requirements. Under a mechanical point of view, the optimum laminates found as result of the first-level problem of the GL-MS2LOS, in terms of macroscopic elastic properties through their polar parameters, must correspond to feasible stacking sequences to be obtained at the end of the second-level problem. According to the formulation proposed by Vannucci in [45] such feasibility conditions, for a quasi-homogeneous orthotropic laminate, can be written only for matrix [A*]:

$$\begin{cases} -R_0 \le R_{0\mathrm{K}}^{\mathrm{A}^*} \le R_0 \;, \\ 0 \le R_1^{\mathrm{A}^*} \le R_1 \;, \\ 2\left(\dfrac{R_1^{\mathrm{A}^*}}{R_1}\right)^2 - 1 - \dfrac{R_{0\mathrm{K}}^{\mathrm{A}^*}}{R_0} \le 0 \;. \end{cases}$$

(18)

These conditions, in terms of the dimensionless design variables introduced in Eq. (13),

15

read:

$$\begin{cases} -1 \le \rho_0 \le 1 \ , \\ 0 \le \rho_1 \le 1 \ , \\ 2 \left(\rho_1 \right)^2 - 1 - \rho_0 \le 0 \ . \end{cases} \tag{19}$$

Naturally, these conditions must be satisfied by the polar parameters describing all the laminates composing the structure: the first two conditions of Eq. (19) are directly used for the definition of the lower and upper bounds of the mechanical design variables (Tab. 7), while the third one is introduced in the problem formulation producing seven further constraint inequalities (g_{12-18}), one for each laminate.

The manufacturing requirements considered are applied by imposing a series of inequalities involving the geometrical design variables:

- Minimum thickness of thin-walled elements:

$$n_{\text{ply}}^{\text{St}-i}, \ n_{\text{ply}}^{\text{Sk}-i}, \ n_{\text{ply}}^{\text{Fr}} \ge 8 \ , \quad \text{with } i = \text{Top, Lat, Bot.} \tag{20}$$

- Minimum length of the interface flange of stiffening components for the installation of rivets:

$$w_3^{\text{St}-i} \ge 14 \text{ mm} \quad \text{with } i = \text{Top, Lat, Bot,}$$
$$w_1^{\text{Fr}} \ge 14 \text{ mm} \ . \tag{21}$$

- Minimum length to thickness ratio of thin-walled elements:

$$w_1^{\text{St}-i}/t^{\text{St}-i} \ge 4 \quad \text{with } i = \text{Top, Lat, Bot,}$$
$$w_3^{\text{St}-i}/t^{\text{St}-i} \ge 3 \quad \text{with } i = \text{Top, Lat, Bot,}$$
$$w_4^{\text{St}-i}/t^{\text{St}-i} \ge 5 \quad \text{with } i = \text{Top, Lat, Bot,}$$
$$w_1^{\text{Fr}}/t^{\text{Fr}} \ge 3 \ ,$$
$$a^{\text{Fr}} \left(\boldsymbol{\xi} \right)/t^{\text{Fr}} \ge 3 \ ,$$
$$b^{\text{Fr}} \left(\boldsymbol{\xi} \right)/t^{\text{Fr}} \ge 3 \ . \tag{22}$$

- Minimum circumferential distance between stringers.

$$pitch^{\text{St}-i} \left(\boldsymbol{\xi} \right) \ge 2 \cdot \left(2 \cdot w_1^{\text{St}-i} + w_3^{\text{St}-i} \right) \quad \text{with } i = \text{Top, Lat, Bot.} \tag{23}$$

Some of these inequalities are directly employed in the definition of the lower and upper bounds of the design variables for the problem at hand, as listed in Tab. 7, whilst the remaining inequalities are stated in the form $l_j \left(\boldsymbol{\xi} \right) \le 0$ and then aggregated into a single constraint using the maximum operator:

$$g_{19} \left(\boldsymbol{\xi} \right) = \max_j \ l_j \left(\boldsymbol{\xi} \right) \le 0 \ . \tag{24}$$

Finally, the optimisation problem can be formulated as a classical CNLPP as follows:

$$\min_{\boldsymbol{\xi}} \mathrm{M}\left(\boldsymbol{\xi}\right) ,$$

subject to: (25)

$$g_i\left(\boldsymbol{\xi}\right) \leq 0 , \qquad \text{with } i = 1, 2, \ldots, 19.$$

The design space of the problem is detailed in Tab. 7.

Design variable	Unit	Lower bound	Upper bound	Step size
w_1^{Fr}	mm	16	50	1
w_3^{Fr}	mm	80	160	2
$n_{\mathrm{ply}}^{\mathrm{Fr}}$	-	8	32	1
$w_1^{\mathrm{St}-i}$	mm	5	30	1
$w_3^{\mathrm{St}-i}$	mm	14	40	1
$w_4^{\mathrm{St}-i}$	mm	14	70	1
$n_{\mathrm{ply}}^{\mathrm{St}-i}$	-	8	32	1.0
$n_{\mathrm{ply}}^{\mathrm{Sk}-i}$	-	8	32	1.0
$n^{\mathrm{Sk}-\mathrm{Top}}$	-	18	38	2
$n^{\mathrm{Sk}-\mathrm{Lat}}$	-	13	36	1
$n^{\mathrm{Sk}-\mathrm{Bot}}$	-	12	26	2
$\rho_0^{\mathrm{St}-i}/\rho_0^{\mathrm{Sk}-i}/\rho_0^{\mathrm{Fr}}$	-	-1	1	*
$\rho_1^{\mathrm{St}-i}/\rho_1^{\mathrm{Sk}-i}/\rho_1^{\mathrm{Fr}}$	-	0	1	*

With i = Top, Lat, Bot.   * Continuous variable.

Table 7: Lower and upper bounds of the design variables.

4.3. Numerical strategy

Problem (25) is a non-convex CNLPP. The total number of design variables is 35, whilst the number of optimisation constraints is 19. For the resolution of problem (25) the GA ERASMUS [26] coupled with both GFEM and LFEMs of the structure has been utilised as optimisation tool to perform the solution search, as illustrated in Fig. 5. The GA ERASMUS has already been successfully applied to solve different kinds of engineering problems, see for example [26, 31, 32, 46–53].

As shown in Fig. 5, for each individual, at each generation, the numerical tool performs global and local FE analyses to calculate the objective function and the optimisation constraints. The FE models are implemented in the ANSYS® environment and their input data are generated by the GA ERASMUS (more details are given in Sec. 5). The GA elaborates the results provided by the GFEM and the LFEMs in order to execute the genetic operations and generate new individuals. These operations are repeated until the GA meets the user-defined convergence criterion. The generic individual of the GA ERASMUS represents a potential solution for the problem at hand. The genotype of the individual for problem (25) is characterised by only one chromosome composed of 35 genes, each one coding a component of the vector of design variables $\boldsymbol{\xi}$.
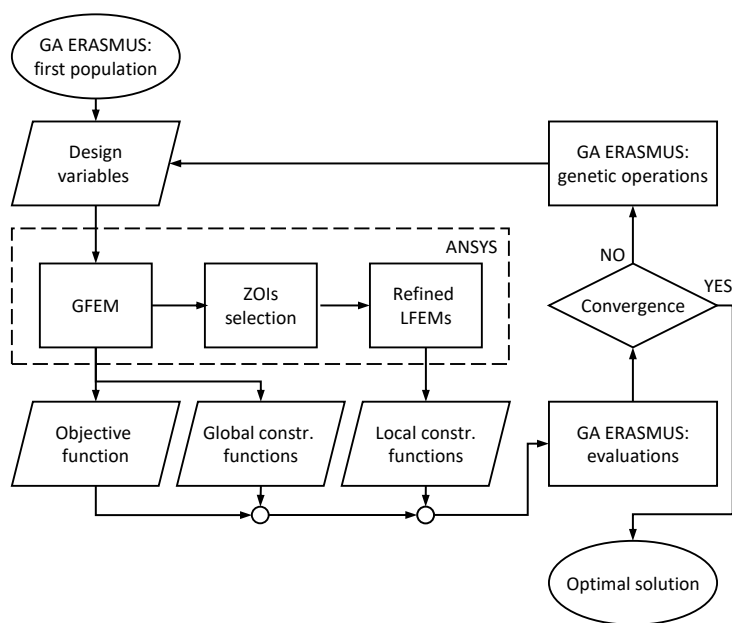
Figure 5: Flowchart of the optimisation process.

5. The global/local finite element modelling approach

As stated above, the FE models integrated in the optimisation process are based on a GL modelling approach. In particular, two different models are created: the GFEM for the assessment of the behaviour of the whole fuselage barrel, and refined LFEMs in order to properly evaluate local responses. LFEMs are created only at the critical ZOIs identified during the global analysis, thus suitable criteria must be developed to accomplish this task.

Both GFEM and LFEMs are fully parametric and are built using the commercial FE code ANSYS®.

5.1. The global finite element model

The global FE model is shown in Fig. 6: it includes seven bays constituting the fuselage barrel. The fuselage skin is modelled with 8-node SHELL281 elements, while frames, stringer, floor beams and struts are modelled with 3-node BEAM189 elements. The beam and shell elements are connected together by node merging. To take into account the actual position of the beam cross-section with respect to the skin, a section offset is applied to beam elements. Shear-tie components are not modelled, but their mechanical effect (the transfer of shear load from the frames to the skin) is ensured by the direct connection between frame and skin elements.

The element type (linear or quadratic) and mesh size have been chosen after performing a sensitivity analysis. The mesh size is controlled by varying the number of element along the portions of frames between two consecutive stringers (while the number of elements in the stringer directions is consequently set to the minimum value ensuring a maximum aspect ratio equal to three for the shell elements). The choice is made by looking for a good compromise between computational time and accuracy in the evaluation of the mechanical responses of the structure at both global and local scales (in fact, the mesh size at the global scale affects the BCs of the local scale analyses, as it is further explained in Sec. 5.2). The details about such a sensitivity analysis are not reported here for the

sake of brevity. As a result of this analysis, a total number of quadratic shell elements varying between 6000 and 8000 (depending on the values of the input parameters) have been used for the GFEM.

Material properties are passed to the model in two different ways. For the shell elements, preintegrated stiffness matrices ([A], [B], [D], [H]) are obtained from the polar parameters through Eqs. (1) and (2) and passed to the model. For beam elements, custom sections are created: for each laminate, an equivalent homogeneous fictitious orthotropic material is defined (this is possible thanks to the quasi-homogeneity hypothesis) and opportunely oriented in the various sectors of the beam cross-section.
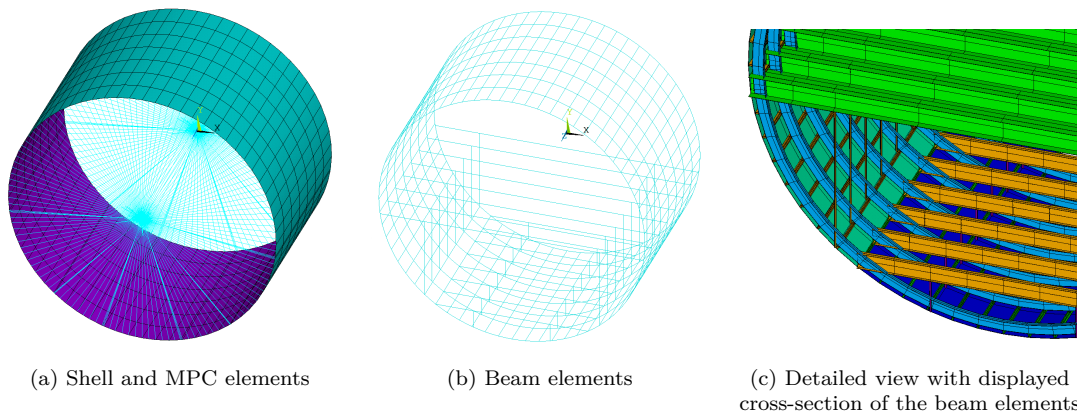

(a) Shell and MPC elements   (b) Beam elements   (c) Detailed view with displayed cross-section of the beam elements

Figure 6: Global FE model.

A master node is created at the centre of sections A and B and linked to the set of "slave" nodes of the corresponding frame by means of MPC184 (multi-point constraint) elements with "rigid beam" behaviour (Fig. 6a). These master nodes are used to apply the BCs presented in Sec. 2.3. In agreement with the hypotheses and the design criteria introduced in Sec. 2.2, only linear static analyses are performed on this model.

Of course, the first bays (from each side of the fuselage barrel) are strongly influenced by edge effects because of the proximity to zones where BCs are applied (i.e. at nodes A and B). Accordingly, only the central bay constitutes the *check zone*, where the results of the analysis are meaningful. Moreover, as explained in Sec. 2.2, the elements adjacent to connection zones (e.g. floor beams to frames connections or the joints between circumferential sectors) are excluded from the check zone, as illustrated in Fig. 7.

Results provided by the GFEM are used for the evaluation of the objective function and all the constraint functions except those related to buckling requirements, i.e. g_9, g_{10} and g_{11}.

5.2. The local finite element models

LFEMs are created to evaluate the first buckling load of the most critical fuselage stiffened panels. This task can be achieved only through a suitably refined FE model able to catch both global and local buckling modes.

Each LFEM includes the same number of stringers and frames, i.e. three and two, respectively, as shown in Fig. 8. The local model presents a suitable extinction zone to mitigate edge effects due to the application of BCs. This extinction zone is half a skin-panel wide and surrounds the check zone, as illustrated in Fig 8. The LFEM is entirely built by using 8-node SHELL281 elements with preintegrated shell sections.

Both frames and stringers are tied to the skin by creating constraint equations between their interface nodes. This allows having an independent mesh size on the different
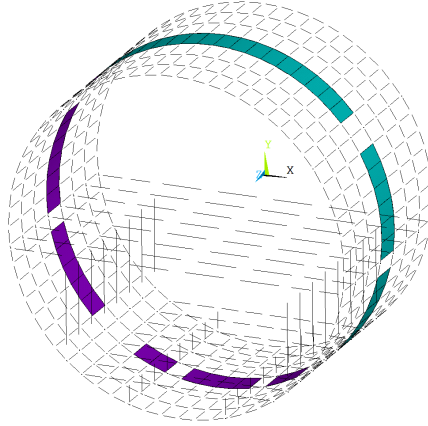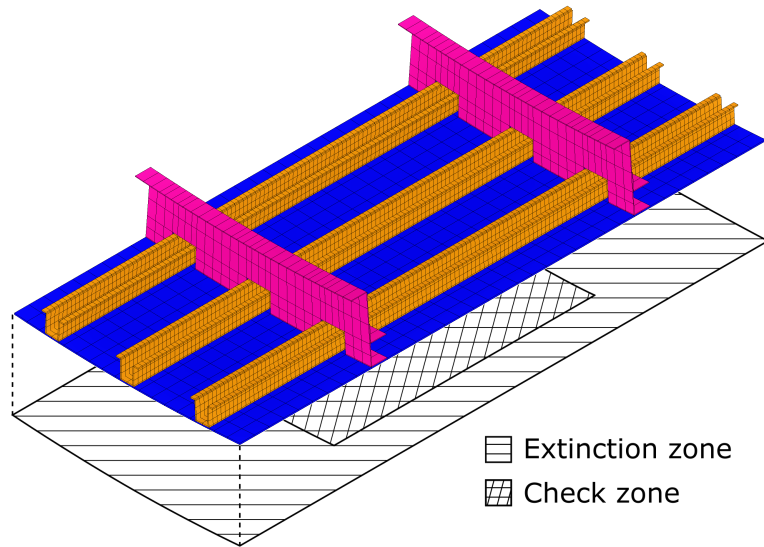
Figure 7: Check zone of the global FE model.

Figure 8: Typical local FE model.

components. Also for the LFEM, the mesh size is the result of a compromise between the accuracy in evaluating the first buckling load of the stiffened panel, which can occur either in the skin or in the flanges of stringers and frames, and the computational time. A sensitivity analysis has been conducted also in this case and it is not reported here for the sake of brevity: the local models have a total number of quadratic shell elements varying from 5000 to 9000 (depending on the values of the input parameters).

Displacement BCs extracted from the results of the global analysis are imposed to all the boundary nodes belonging to the skin of the local FE model.

To transfer the BCs to stringers and frames, for each ending cross-section, a master node is extracted from the skin boundary nodes located at the interface between the beam reference axis and the skin in the GFEM. The coordinates of this set of master nodes are recorded and passed to the LFEM (for each region of the fuselage barrel). Then these nodes are selected and connected to those belonging to the corresponding stringer/frame ending cross-section by means of MPC184 elements with "rigid beam" behaviour, ensuring in this way the kinematic compatibility between global and local models, see Fig. 9.

The LFEM is built for each sector of the fuselage barrel (bottom, top and lateral).
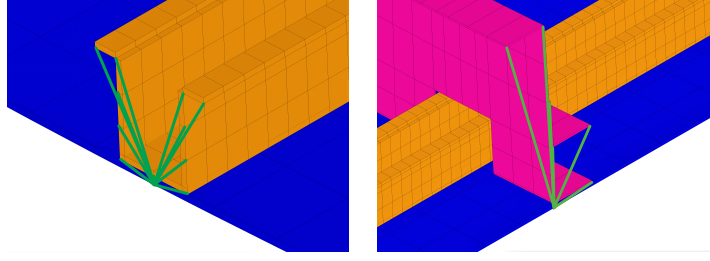
Figure 9: Detail of the ending cross-section of the stiffening components in the local FE model.

An eigenvalue buckling analysis is performed on the local models, and the lowest positive eigenvalue, $\lambda(\boldsymbol{\xi})$, is retrieved as output.

5.3. ZOIs identification criteria and information transfer between global and local models

In the presented GL-MS2LOS, the fewest number of local models is checked in order to keep the computational time as low as possible. To this purpose, specific criteria have been introduced and applied to the post-processing of results coming from the GFEM in order to identify the most critical ZOIs around which LFEMs are automatically generated. For each circular sector belonging to the check zone, only one ZOI is identified and analysed.

As discussed in Secs. 2.3 and 4.2, the buckling-related constraints are evaluated for LC4 and LC5 (see Tab. 6). These LCs are obtained by scaling $\mathrm{BLC_{1g}}$ by means of a suitable load factor. Under $\mathrm{BLC_{1g}}$, the stiffened panels in the top and bottom sectors are mostly subject to stress in the longitudinal direction, as shown in Fig. 10. Therefore,
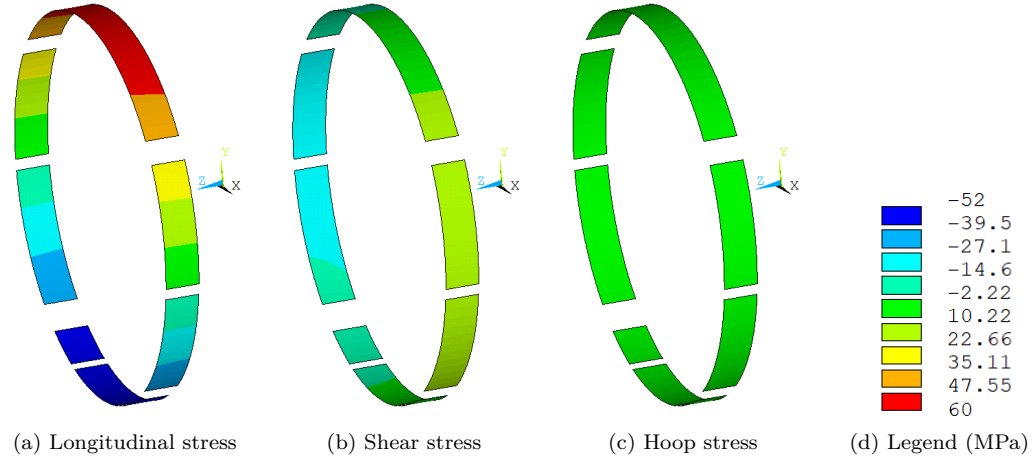

(a) Longitudinal stress   (b) Shear stress   (c) Hoop stress   (d) Legend (MPa)

Figure 10: Stress distribution in the skin-panels in the check zone at $\mathrm{BLC_{1g}}$.

top and bottom ZOIs are identified by looking for the *basic-panel* (BP), i.e. the assembly composed of a stringer plus half of the adjacent skin-panels, that withstands the lowest (compressive, hence negative) average longitudinal force per unit width, $\mathrm{N_l^{BP}}$, computed , for the generic LC, as

$$\mathrm{N_l^{BP}} = \frac{\mathrm{F^{St}} + \int_{-w^{SP}/2}^{w^{SP}/2} \int_0^{t^{Sk}} \sigma_l^{Sk} \, \mathrm{d}z \, \mathrm{d}y}{w^{SP}} \ , \tag{26}$$

where $\mathrm{F^{St}}$ is the axial tensile force in the stringer, w^{SP} is the width, in the hoop direction, of the skin panel and σ_l^{Sk} is the longitudinal stress in the skin.

On the other hand, the panels in the lateral sector are subject to biaxial loads corresponding to a combination of mainly shear and longitudinal stress; the latter varying from tensile to compression depending on the position of the considered stiffened panel (see Fig. 10). Accordingly, a different criterion is used for the lateral sector: the ZOI is identified by looking for the most critical skin-panel with respect to the buckling strength. An estimation of the buckling load is computed for each skin-panel in the check zone using the analytical formula for a simply supported plate with the same dimensions of the analysed skin-panel, i.e. a in the longitudinal direction and b in the hoop one, and subject to the same bi-axial stress field given by the membrane forces per unit width N_x, N_y, and N_{xy}. Under the hypothesis that such a plate buckles with an out-of-plane displacement field described by

$$w(x, y) = a_{mn} \sin \frac{m\pi x}{a} \sin \frac{n\pi y}{b} \; , \tag{27}$$

the related buckling eigenvalue can be computed as [54]

$$\lambda_b = \pi^2 \frac{D_{xx}(m/a)^4 + 2(D_{xy} + 2D_{ss})(m/a)^2(n/b)^2 + D_{yy}(n/b)^4}{N_x(m/a)^2 + N_y(n/b)^2 + N_{xy}(mn/ab)} \; , \tag{28}$$

where the x and y directions correspond to the longitudinal and hoop ones; D_{xx}, D_{xy}, D_{yy} and D_{ss} are the components of the bending stiffness matrix [D] of the laminate in Voigt's notation.

The estimation of the first buckling factor for the skin-panel can be finally obtained as

$$\lambda_{cb} = \min_{m,n} (\lambda_b) \; . \tag{29}$$

Therefore, the skin-panel showing the minimum λ_{cb} identifies the lateral ZOI.

As already stated, the displacement field resulting from the GFEM is used to define the BCs for the LFEMs. To this purpose, for each LC, the nodal displacements of the GFEM are interpolated using the shape functions of the elements in the GFEM at the location of the boundary nodes of the LFEM. The logical flow of the process that goes from the global FE analysis to the local one is given in Fig. 11.
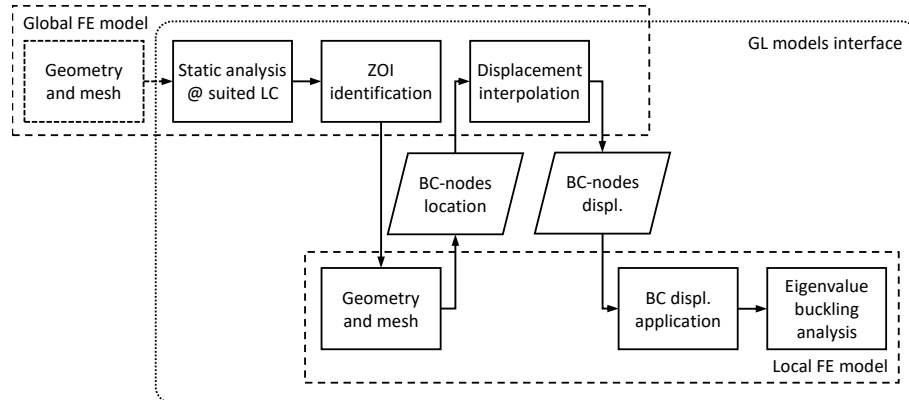

Figure 11: Interaction scheme between global and local finite element models.

6. Numerical results

The parameters of the GA ERASMUS used to perform the solution search for problem (25) are listed in Tab. 8. As far as the optimisation constraints are concerned, they have been handled through the Automatic Dynamic Penalisation (ADP) method [55]. Further details on the optimisation tool and its parameters can be found in [26].

Property	Value
N. of populations	2
N. of individuals per population	400
N. of chromosomes	1
N. of genes	35
Stop criterion	Fixed generations (150)
Crossover probability	0.85
Mutation probability	0.01
Selection operator	Tournament
Fitness pressure	1
Elitism operator	Active
Isolation time	Infinite

Table 8: Parameters of the GA ERASMUS used for the solution search.

The whole optimisation process requires a computational time of approximately 45 days (i.e. around 70 s for global and local FE analyses for the generic point in the design space) when four cores of a machine with an Intel Xeon E5-2697v2 processor (2.70-3.50 GHz) are dedicated to the ANSYS solver and the two populations are run in parallel. However, computational time could be easily reduced by performing in parallel the FE calculations of the different individuals of the same population. Indeed, because most of the computational time is spent into the FE analyses, and each analysis is independent to the others, the overall optimisation time is inversely proportional to the number of FE analyses performed in parallel.

Three individuals of the last generation of the optimisation are analysed, denoted as S1, S2 and S3, S1 being the optimum solution. The complete set of performances, in terms of constraint and objective functions, for these individuals and the associated design variables values are listed in Tabs. 9 and 10, respectively. A quick glance to these results suffices to infer that, due the non-convex nature of problem (25), the GA finds almost equivalent optimal solutions, e.g. S1, S2 and S3, different in term of design variables, that still respect all the constraints and that have comparable values of the objective function. Moreover, a significant number of pseudo-optimal solutions exists that are nearly identical to solution S1 and that are not reported here for the sake of brevity.

As reported in Tab. 9, the constraint g_1 (related to the stiffness requirement) clearly reveals the most restrictive one for the three solutions.

Concerning the retained optimal solution, i.e. S1, from Tab. 10 one can notice that some of the variables are located at the bounds of the respective intervals, see Tab. 7. In particular, the number of skin-panels, in the three circumferential sectors are close to their upper bounds. This suggests that an even lighter solution, with closer stringers, may be found by extending the bounds of such variables.

It is noteworthy that the optimal values of the laminate polar parameters of the skin in the three sectors (small values of ρ_1 and bigger negative values of ρ_0) describe laminates characterised by an almost perfect *square symmetry* with the main orthotropic axes oriented at $\pm 45°$ with respect to the fuselage longitudinal axis. On the other hand, the optimum laminates of the frames and of the stringers, have a standard orthotropic behaviour, consequence of the bigger values of ρ_1, with the main orthotropic axis alligned

23

Function		S3	S2	S1*
g_1	(stiffness)	-0.039	-0.062	-0.050
g_2	(stiffness)	-0.301	-0.244	-0.276
g_3	(strength)	-0.104	-0.108	-0.100
g_4	(strength)	-0.592	-0.614	-0.573
g_5	(strength)	-0.463	-0.479	-0.544
g_6	(strength)	-0.463	-0.452	-0.284
g_7	(strength)	-0.553	-0.551	-0.500
g_8	(strength)	-0.351	-0.371	-0.367
g_9	(buckling)	-0.303	-0.122	-0.258
g_{10}	(buckling)	-0.139	-0.128	-0.126
g_{11}	(buckling)	-0.189	-0.289	-0.410
g_{12-18}	(laminate feasibility)	< 0.000	< 0.000	< 0.000
g_{19}	(manufacturability)	< 0.000	< 0.000	< 0.000
M [kg]		$529\,(-38\%)^\dagger$	$521\,(-38\%)^\dagger$	$506\,(-40\%)^\dagger$

* Retained optimal solution
$\dagger$ With respect to $M^{REF} = 847$ kg

Table 9: Comparison of the values of the constraint and objective functions relative to different individuals.

with the beams longitudinal direction. This can be visualised, for example, by plotting the polar diagram of the first component of matrix $[A]^*$ for the bottom skin laminate and for the bottom stringer one of solution S1, as shown in Fig. 12. For a deeper insight on these aspects, the reader is addressed to [23, 24].
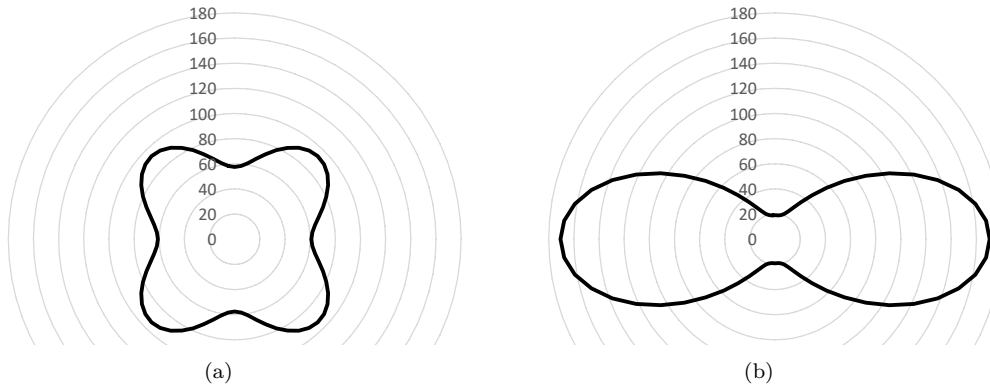

Figure 12: Polar diagram of the first component of matrix $[A]^*$ in GPa for the laminates of the bottom skin (a) and the bottom stringer (b) for solution S1. The horizontal direction represents the fuselage longitudinal axis.

The buckling mode of the identified critical stiffened panel, for each one of the three sectors for solution S1, is illustrated in Fig. 13. It can be noticed that the stringers and the skin buckle simultaneously in the lateral and bottom sector. This is in agreement with the well-established aeronautical design criterion that the maximum structural efficiency (in terms of best compromise between minimum weight and maximum buckling load) for stiffened structures is reached when their components buckle at the same load [56]. This does not occur for the top sectors stiffened panels, where the stringers appear to be over-sized, with respect to buckling, and are not involved into the buckling deformation. This last point suggests that a margin of improvement for the optimisation of these components is still possible.

Finally, in Tab. 9, the mass of solution S1 is compared with the mass of the metallic solution RES (i.e. 847 kg): a weight saving of 40% has been obtained which can be interpreted as a numerical proof of the effectiveness of the GL-MS2LOS. Therefore, the

Variable	S3			S2			S1*		
	Top	Lat.	Bot.	Top	Lat.	Bot.	Top	Lat.	Bot.
w_1^{Fr} [mm]		20.0			19.0			17.0	
w_3^{Fr} [mm]		97.0			86.0			85.0	
t^{Fr} [mm]		1.125			1.125			$1.000^\dagger$	
ρ_0^{Fr} [-]		0.656			0.667			0.684	
ρ_1^{Fr} [-]		0.415			0.459			0.467	
w_1^{St} [mm]	10.0	6.0	15.0	12.0	7.0	14.0	13.0	6.0	12.0
w_3^{St} [mm]	39.0	39.0	38.0	39.0	$40.0^\dagger$	34.0	35.0	39.0	39.0
w_4^{St} [mm]	18.0	27.0	63.0	16.0	26.0	50.0	26.0	27.0	29.0
t^{St} [mm]	1.500	$1.000^\dagger$	3.250	1.625	$1.000^\dagger$	3.375	1.625	$1.000^\dagger$	2.750
ρ_0^{St} [-]	0.627	0.946	0.864	0.728	0.922	0.842	0.758	0.883	0.940
ρ_1^{St} [-]	0.275	0.880	0.738	0.230	0.796	0.751	0.285	0.834	0.884
t^{Sk} [mm]	1.375	1.500	1.375	1.375	1.625	1.500	1.250	1.500	1.500
ρ_0^{Sk} [-]	-0.952	-0.757	-0.936	-0.957	-0.816	$-1.000^\dagger$	-0.940	-0.898	-0.867
ρ_1^{Sk} [-]	0.029	0.015	0.014	0.030	0.012	0.008	0.092	0.024	0.021
n^{Sk} [-]	34	32	24	32	32	22	36	$36^\dagger$	$26^\dagger$

* Retained optimal solution † Values at the bounds of the design space (see Tab. 7)

Table 10: Design variables values for optimal individuals at the last generation.

proposed approach allows finding an optimal configuration of the composite fuselage barrel satisfying the full set of design requirements, without introducing simplifying hypotheses into the design strategy at each characteristic scale.

7. Conclusions

A multi-scale optimisation strategy, denoted as GL-MS2LOS, for designing composite thin-walled structures has been presented in this work. Such strategy has been formulated by integrating a dedicated global-local modelling approach into the MS2LOS, allowing in this way a proper optimisation of big composite thin-walled structures where a *global macroscopic* scale and a *local macroscopic* one can be identified, as those commonly used in the aerospace industry.

As usual for this type of structures, the design problem is formulated as a CNLPP involving requirements of different nature. In particular, some requirements involve the structure response, at different scales, under various loading conditions. To this purpose, the GL-MS2LOS aims at proposing a very general formulation of the design problem, without introducing simplifying hypotheses and by considering, as design variables, the full set of geometric and mechanical parameters defining the behaviour of the composite structure at each pertinent scale.

In the framework of the MS2LOS, the problem is split into two subsequent optimisation problems. The first-level problem represents the true structural optimisation and focuses on the macroscopic scale (both global and local models are involved). At this scale, the laminates composing the structure are considered as equivalent anisotropic single layers whose macroscopic behaviour is described in terms of their polar parameters. The optimisation is performed by including both geometrical and macroscopic mechanical variables describing the structure into the problem formulation, without making simplifying hypotheses neither on the nature of the stacking sequences of the laminates nor on

(a) Lateral sector panel

(b) Top sector panel
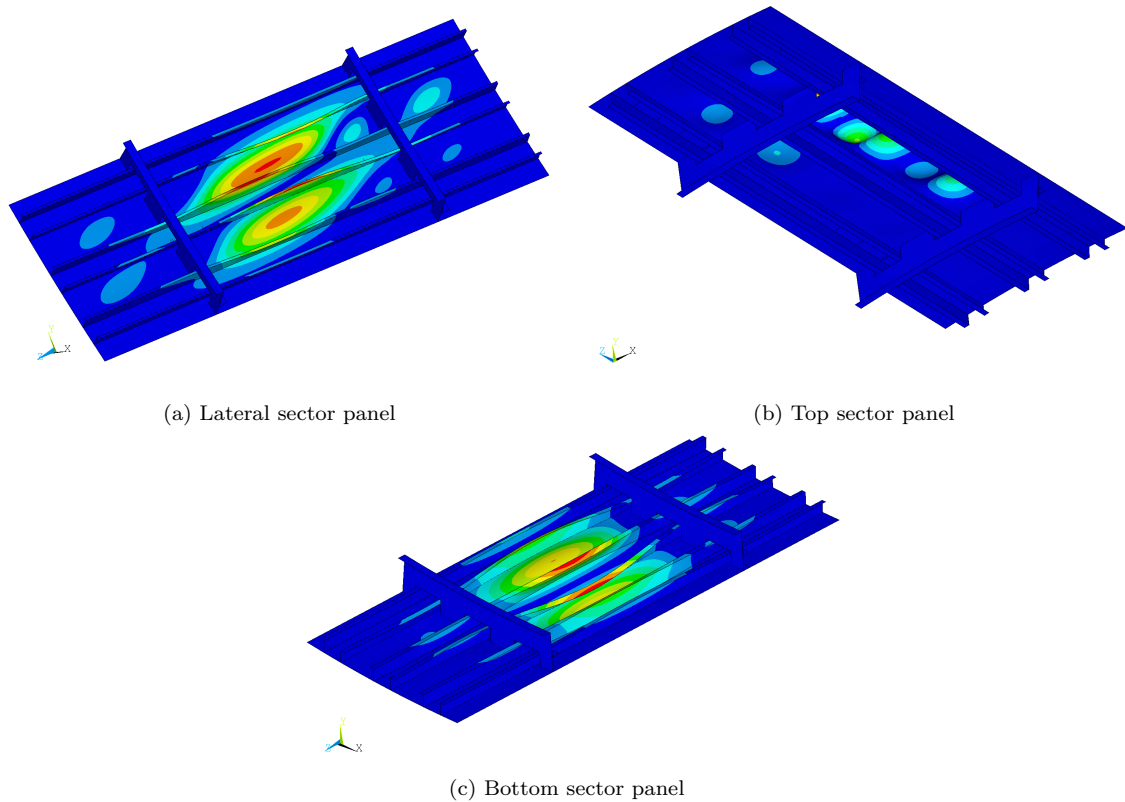
(c) Bottom sector panel

Figure 13: Normalised displacement field for the first buckling mode of the local models for the optimum solution.

the other design variables. The second-level optimisation problem, not presented in this paper, is devoted to the retrieval of the laminates stacking sequences corresponding to the sets of optimum polar and geometrical parameters found at the first level.

The GL modelling approach is integrated at the first level of the MS2LOS: fully parametric FE models are created at both the global and the local macroscopic scales for the evaluation of the most relevant phenomena. A coherent information transfer between these models is ensured by implementing a sub-modelling GL approach: BCs of the local models are directly extracted, in terms of displacements, from the results of the global analysis and properly transferred to the local FE model. Local FE models are automatically created only for critical ZOIs which are identified, by means of opportune criteria, during the global analysis. The solution search for the first-level multi-scale CNLPP is performed by interfacing the GFEM and the LFEMs of the structure with the GA ERASMUS developed at the I2M laboratory in Bordeaux.

By employing a GL modelling approach, most of the limitations of other well-established strategies are overcome; namely more accurate results than those found by means of simplified analytical models (for the assessment of the mechanical response of the structure) can be obtained. Furthermore, the load redistribution due to changes of the variables at the local scale is automatically accounted for. Finally, the whole process, once set, is fully automated and does not need the user intervention.

The effectiveness of the presented GL-MS2LOS is proven on a meaningful design case: the least-weight design of a composite fuselage barrel of a wide-body aircraft. In the considered test case, a limited, yet representative, set of loading conditions and design criteria is considered. Nevertheless, further criteria and load cases could be easily introduced in

26

the general framework of the presented design strategy.

The obtained optimum composite fuselage is compared to an analogous aluminium one previously optimised by the authors employing a similar GL optimisation strategy and subject to equivalent design criteria: a weight saving of about 40% is obtained while respecting the full set of design constraints. This result is very promising, even more if considering that the floor beams and the struts have not been included in the design process.

These results encourage research activity in this direction. As far as perspectives of this work are concerned, ongoing research is focused on the formulation of post-buckling requirements, on the integration of blending constraints between adjacent skin laminates and on the improvement of the strategy allowing to design composite thin-walled structures made of variable angle tow laminates.

Appendix A. Analytical expression of the laminate strength and stiffness matrices and vectors

According to the generic laminate stacking scheme of Fig. A.1, the analytical expression of the laminate stiffness matrices $[A]$, $[B]$, $[D]$ and $[H]$ is given in Eq. (A.1), while that of the laminate strength matrices $[G_A]$, $[G_B]$, $[G_D]$, $[G_H]$ and vectors $\{g_A\}$ and $\{g_D\}$ is provided in Eq. (A.2).
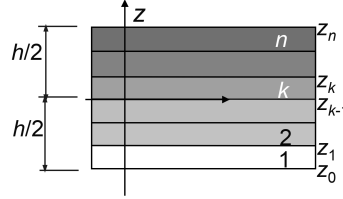

Figure A.1: Laminate stacking scheme.

$$
\begin{aligned}
[A] &= \sum_{k=1}^{n} (z_k - z_{k-1}) \left[Q^{\text{in}}(\delta_k) \right], \quad [B] = \frac{1}{2} \sum_{k=1}^{n} \left(z_k^2 - z_{k-1}^2 \right) \left[Q^{\text{in}}(\delta_k) \right], \\
[D] &= \frac{1}{3} \sum_{k=1}^{n} \left(z_k^3 - z_{k-1}^3 \right) \left[Q^{\text{in}}(\delta_k) \right], \quad [H] = \sum_{k=1}^{n} (z_k - z_{k-1}) \left[Q^{\text{out}}(\delta_k) \right],
\end{aligned}
\tag{A.1}
$$

$$
\begin{aligned}
[G_A] &= \sum_{k=1}^{n} (z_k - z_{k-1}) \left[G^{\text{in}}(\delta_k) \right], \quad [G_B] = \frac{1}{2} \sum_{k=1}^{n} \left(z_k^2 - z_{k-1}^2 \right) \left[G^{\text{in}}(\delta_k) \right], \\
[G_D] &= \frac{1}{3} \sum_{k=1}^{n} \left(z_k^3 - z_{k-1}^3 \right) \left[G^{\text{in}}(\delta_k) \right], \quad [G_H] = \sum_{k=1}^{n} (z_k - z_{k-1}) \left[G^{\text{out}}(\delta_k) \right], \quad \text{(A.2)} \\
\{g_A\} &= \sum_{k=1}^{n} (z_k - z_{k-1}) \left\{ g^{\text{in}}(\delta_k) \right\}, \quad \{g_D\} = \frac{1}{2} \sum_{k=1}^{n} \left(z_k^2 - z_{k-1}^2 \right) \left\{ g^{\text{in}}(\delta_k) \right\}.
\end{aligned}
$$

The expression of the above matrices and vectors in terms of the related polar parameters can be found in [23, 24, 41].

Data availability

The raw/processed data required to reproduce these findings cannot be shared at this time as the data also forms part of an ongoing study.

References

References

[1] H. Ghiasi, D. Pasini, L. Lessard, Optimum stacking sequence design of composite materials Part I: Constant stiffness design, Composite Structures 90 (2009) 1–11.

[2] M. Albazzan, R. Harik, B. Tatting, Z. Gürdal, Efficient design optimization of non-conventional laminated composites using lamination parameters: A state of the art, Composite Structures 209 (2019) 362 – 374.

[3] S. Adali, V. Verijenko, M. Walker, Optimal laminate configurations with symmetric lay-ups for maximum postbuckling stiffness, Composites Engineering 4 (11) (1994) 1119 – 1127.

[4] R. Haftka, J. Walsh, Stacking-sequence optimization for buckling of laminated plates by integer programming, AIAA Journal 30 (3) (1992) 814–819.

[5] R. Le Riche, R. Haftka, Optimization of laminate stacking sequence for buckling load maximization by genetic algorithm, AIAA Journal 31 (5) (1993) 951–956.

[6] F. Aymerich, M. Serra, Optimization of laminate stacking sequence for maximum buckling load using the ant colony optimization (ACO) metaheuristic, Composites Part A: Applied Science and Manufacturing 39 (2) (2008) 262–272.

[7] F. Irisarri, D. Bassir, N. Carrere, J. Maire, Multiobjective stacking sequence optimization for laminated composite structures, Composites Science and Technology 69 (7-8) (2009) 983–990.

[8] F. Irisarri, F. Laurin, F. Leroy, J. Maire, Computational strategy for multiobjective optimization of composite stiffened panels, Composite Structures 93 (3) (2011) 1158–1167.

[9] C. Bisagni, R. Vescovini, A fast procedure for the design of composite stiffened panels, The Aeronautical Journal 119 (1212) (2015) 185–201.

[10] U.S. Department of Defense, Military Handbook - MIL-HDBK-17-3F: Composite Materials Handbook, Volume 3 - Polymer Matrix Composites Materials Usage, Design and Analysis (2002).

[11] R. Jones, Mechanics of composite materials, McGraw-Hill, 1975.

[12] S. Tsai, N. Pagano, Invariant properties of composite materials., Tech. rep., Air force materials lab Wright-Patterson AFB Ohio (1968).

[13] S. Tsai, T. Hahn, Introduction to composite materials, Technomic, 1980.

[14] M. Bloomfield, J. Herencia, P. Weaver, Optimisation of anisotropic composite plates incorporating non-conventional ply orientations, in: 49th AIAA/ASME/ASCE/AHS/ASC Structures, Structural Dynamics, and Materials Conference, 16th AIAA/ASME/AHS Adaptive Structures Conference, 10th AIAA Non-Deterministic Approaches Conference, 9th AIAA Gossamer Spacecraft Forum, 4th AIAA Multidisciplinary Design Optimization Specialists Conference, 2008, p. 1918.

[15] S. Liu, Y. Hou, X. Sun, Y. Zhang, A two-step optimization scheme for maximum stiffness design of laminated plates based on lamination parameters, Composite Structures 94 (12) (2012) 3529–3537.

[16] J. Herencia, P. Weaver, M. Friswell, Initial sizing optimisation of anisotropic composite panels with T-shaped stiffeners, Thin-Walled Structures 46 (4) (2008) 399–412.

[17] K. Bramsiepe, V. Handojo, M. Meddaikar, M. Schulze, T. Klimmek, Loads and structural optimisation process for composite long range transport aircreft configuration, AIAA Aviation Forum, Atlanta, Georgia, 2018.

[18] W. J. Vankan, R. Maas, S. Grihon, Efficient optimisation of large aircraft fuselage structures, The Aeronautical Journal 118 (1199) (2014) 31–52.

[19] W. Vankan, B. Noordman, K. Kueres, High and low fidelity finite element modelling in aircraft composite fuselage structural analysis and optimisation, Technical report 2013-197, National Aerospace Laboratory NLR (2014).

[20] S. Grihon, L. Krog, D. Bassir, Numerical Optimization applied to structure sizing at AIRBUS: A multi-step process, International Journal for Simulation and Multidisciplinary Design Optimization 3 (4) (2009) 432–442.

[21] S. Venkataraman, R. Haftka, Structural optimization complexity: what has moore's law done for us?, Structural and Multidisciplinary Optimization 28 (6) (2004) 375–387.

[22] G. Verchery, Les invariants des tenseurs d'ordre 4 du type de l'élasticité, Proc. of colloque Euromech 115, VIllard-de-Lans, (France), 1979.

[23] M. Montemurro, An extension of the polar method to the first-order shear deformation theory of laminates, Composite Structures 127 (2015) 328–339.

[24] M. Montemurro, Corrigendum to "an extension of the polar method to the first-order shear deformation theory of laminates" [compos. struct. 127 (2015) 328-339], Composite Structures 131 (2015) 1143–1144.

[25] M. Montemurro, The polar analysis of the third-order shear deformation theory of laminates, Composite Structures 131 (2015) 775–789.

[26] M. Montemurro, A contribution to the development of design strategies for the optimisation of lightweight structures. HDR thesis, Université de Bordeaux, http://hdl.handle.net/10985/15155, Bordeaux, France, 2018.
URL http://hdl.handle.net/10985/15155

[27] M. Montemurro, A. Catapano, D. Doroszewski, A multi-scale approach for the simultaneous shape and material optimisation of sandwich panels with cellular core, Composites Part B 91 (2016) 458–472.

[28] M. Montemurro, A. Catapano, On the effective integration of manufacturability constraints within the multi-scale methodology for designing variable angle-tow laminates, Composite Structures 161 (2017) 145–159.

[29] M. Montemurro, A. Pagani, G. Fiordilino, J. Pailhès, E. Carrera, A general multi-scale two-level optimisation strategy for designing composite stiffened panels, Composite Structures 201 (2018) 968 – 979.

[30] M. Montemurro, A. Catapano, A general B-Spline surfaces theoretical framework for optimisation of variable angle-tow laminates, Composite Structures 209 (2019) 561 – 578.

[31] E. Panettieri, M. Montemurro, A. Catapano, Blending constraints for composite laminates in polar parameters space, Composites Part B: Engineering 168 (2019) 448 – 457.

[32] M. Montemurro, M. Izzi, J. El-Yagoubi, D. Fanteria, Least-weight composite plates with unconventional stacking sequences: Design, analysis and experiments, Journal of Composite Materials 53 (16) (2019) 2209–2227.

[33] C. Sun, K. Mao, A global-local finite element method suitable for parallel computations, Computers & Structures 29 (2) (1988) 309–315.

[34] K. Mao, C. Sun, A refined global-local finite element analysis method, International Journal for Numerical Methods in Engineering 32 (1) (1991) 29–43.

[35] J. Whitcomb, Iterative global/local finite element analysis, Computers & Structures 40 (4) (1991) 1027–1031.

[36] N. Cormier, B. Smallwood, G. Sinclair, G. Meda, Aggressive submodelling of stress concentrations, International Journal for Numerical Methods in Engineering 46 (6) (1999) 889–909.

[37] L. Boni, D. Fanteria, Finite-element-based assessment of analytical methods for the design of fuselage frames, Proceedings of the Institution of Mechanical Engineers, Part G: Journal of Aerospace Engineering 220 (5) (2006) 387–398.

[38] B. Zhang, R. Dai, W. Ma, H. Wu, L. Jiang, C. Yan, Y. Zhang, Analysis and design of carbon fibre clamping apparatus for replacement of insulator strings in ultra-high voltage transmission line, The Journal of Engineering 2019 (16) (2019) 2212–2215.

[39] Metallic materials and elements for aerospace vehicle structures MIL-HDBK-5j, Tech. rep., Departement of defence - United States of America (2003).

[40] Certification specifications and acceptable means of compliance for large aeroplanes CS-25, Tech. rep., Official Publication of the European Aviation Safety Agency (2018).

[41] A. Catapano, M. Montemurro, On the correlation between stiffness and strength properties of anisotropic laminates, Mechanics of Advanced Materials and Structures 26 (8) (2019) 651–660.

[42] P. Vannucci, Plane anisotropy by the polar method, Meccanica 40 (2005) 437–454.

[43] J. N. Reddy, Mechanics of composite laminated plates and shells: theory and analysis, Boca Raton, FL: CRC Press, 2003.

[44] S. Tsai, E. Wu, A General Theory of Strength for Anisotropic Materials, Journal of Composite Materials 5 (1) (1971) 58–80.

[45] P. Vannucci, A note on the elastic and geometric bounds for composite laminates, Journal of Elasticity 112 (2013) 199–215.

[46] G. Costa, M. Montemurro, J. Pailhès, A General Hybrid Optimization Strategy for Curve Fitting in the Non-Uniform Rational Basis Spline Framework, Journal of Optimization Theory and Applications 176 (1) (2018) 225–251.

[47] G. Bertolino, M. Montemurro, G. D. Pasquale, Multi-scale shape optimisation of lattice structures : an evolutionary-based approach, International Journal on Interactive Design and Manufacturing (2019 (In press)).

[48] Y. Audoux, M. Montemurro, J. Pailhes, A surrogate model based on Non-Uniform Rational B-Splines hypersurfaces, Procedia CIRP 70 (2018) 463 – 468, 28th CIRP Design Conference 2018, 23-25 May 2018, Nantes, France.

[49] M. Montemurro, A. Catapano, On the effective integration of manufacturability constraints within the multi-scale methodology for designing variable angle-tow laminates, Composite Structures 161 (2017) 145 – 159.

[50] L. Cappelli, G. Balokas, M. Montemurro, F. Dau, L. Guillaumat, Multi-scale identification of the elastic properties variability for composite materials through a hybrid optimisation strategy, Composites Part B: Engineering 176 (2019 (in press)).
URL https://doi.org/10.1016/j.compositesb.2019.107193

[51] A. Catapano, M. Montemurro, J.-A. Balcou, E. Panettieri, Rapid prototyping of variable angle-tow composites, Aerotecnica Missili & Spazio (2019).
URL https://doi.org/10.1007/s42496-019-00019-0

[52] L. Cappelli, M. Montemurro, F. Dau, L. Guillaumat, Multi-scale identification of the viscoelastic behaviour of composite materials through a non-destructive test, Mechanics of Materials 137 (2019 (in press)) 103137.
URL https://doi.org/10.1016/j.mechmat.2019.103137

[53] M. Montemurro, A. Vincenti, P. Vannucci, Design of elastic properties of laminates with minimum number of plies, Mechanics of Composite Materials 48 (2012) 369–390.

[54] A. R. M. Rao, N. Arvind, A scatter search algorithm for stacking sequence optimisation of laminate composites, Composite Structures 70 (4) (2005) 383 – 402.

[55] M. Montemurro, A. Vincenti, P. Vannucci, The automatic dynamic penalisation method (ADP) for handling constraints with genetic algorithms, Computer Methods in Applied Mechanics and Engineering 256 (2013) 70–87.

[56] G. Gerard, Minimum weight analysis of compression structures, New York University Press, 1956.